PNAS

Supporting Information for

Genetic and phenotypic profiling of single living circulating tumour cells from patients with microfluidics

Zaizai Dong,[#] Yusen Wang,[#] Gaolian Xu,[#] Bing Liu,[#] Yang Wang, Julien Reboud, Pawel Jajesniak, Shi Yan, Pingchuan Ma, Feng Liu, Yuhao Zhou, Zhiyuan Jin, Kuan Yang, Zhaocun Huang, Minglei Zhuo, Bo Jia, Jian Fang, Panpan Zhang, Nan Wu,* Mingzhu Yang,* Jonathan M. Cooper*, Lingqian Chang*

* Corresponding authors. Email: Jon.Cooper@glasgow.ac.uk (J.M.C.); lingqianchang@buaa.edu.cn (L.C.); yixin051@163.com (M.Y.); nanwu@bjmu.edu.cn (N.W.)

This PDF file includes:

Supplementary methods
Figures S1 to S16
Tables S1 to S10

Other supporting materials for this manuscript include the following:

Movies S1 to S8

Supplementary methods

Fabrication of the WBC-Removal Layer and CTC-Capture Layer. Briefly, the negative photoresist was spin-coated on a clean silicon wafer (WBC-Removal Layer, SU8-2075, 200 μm; CTC-Capture Layer, SU8-2025, 40 μm). After a soft bake, the silicon wafer was exposed to ultraviolet light under the mask by a lithography machine (URE-2000/17, Institute of Optics and Electronics, Chinese Academy of Sciences). Subsequently, the uncured photoresist on the silicon wafer was washed by the negative developer solution. The obtained microstructure on silicon wafer was used as a mold to fabricate the WBC-Removal Layer and CTC-Capture Layer by polydimethylsiloxane (PDMS).

Preparation of CD45-MBs. For the preparation of CD45-MBs, 100 μL streptavidin-modified magnetic beads were mixed with 10 μL biotin-labeled anti-CD45 antibody and incubated at 37 °C for 2 h. After centrifugation at 2000 rpm for 5 min, the magnetic beads were washed with phosphate buffer solution (PBS, Corning) three times. Then, the CD45-MBs were incubated in 5% (w/v) Bovine Serum Albumin (BSA, Biodee) in PBS for 30 min. The obtained CD45-MBs were centrifuged at 2000 rpm for 5 min and washed with PBS three times. Finally, the CD45-MBs were resuspended in 100 μL PBS buffer supplemented with 1% BSA and stored at 4 °C.

Cell culture. The human lung adenocarcinoma cell lines A549, HCC827, human embryonic kidney cell line 293FT, human T lymphocyte Jurkat cell line, and human T lymphocytic leukemia cell line HuT-78 were obtained from the National Platform of Experimental Cell Resources. A549 cells and 293FT cells were cultured in DMEM containing FBS (10%) and penicillin-streptomycin (100 units/mL). HCC827 cells, Jurkat T cells and HuT-78 cells were cultured in RPMI 1640 medium containing FBS (10%) and penicillin-streptomycin (100 units/mL). The above cells were cultured at 5% CO_2 and 37 °C.

Gene regulation of cells. For up-regulating PD-L1 expression, a PD-L1 DNA plasmids (purchased from Keweichuang Biotechnology Co., Shanghai) was delivered into A549 cells by lipo3000 (L3000015, Invitrogen), following a standard protocol of the plasmid transfection (*1, 2*). Briefly, 2 μL lipofectamine 3000 and 3 μL P3000 was diluted with 50 μL opti-MEM medium (31985070, Gibco), respectively. 1 μg PD-L1 plasmid was added into P3000 and then incubated with lipofectamine 3000 for 15 min at 25 °C. After the cells proliferated to be 70% confluent, the above mixture of PD-L1 plasmid and lipofectamine 3000 was added into the cell medium and incubated at 37 °C for 6 h. After that, the cells were incubated into fresh medium for 24 h. For downregulation of CK RNA, HCC827 cells were incubated with 70 pmol of CK SiRNA (Sense: 5'-UCGAGACACGUGAUGGGAAGCUGGU-3'; Antisense 5'-ACCAGCUUCCCAUCACGUGUCUCGA-3') and 8 μL of transfection reagent (GenePharma) for 36 h. For downregulation of PD-L1 RNA, A549 cells were incubated with PD-L1 SiRNA (Sense: 5'-GAUGAGGAUAUUUGCUGUCUUUAUA-3'; Antisense 5'-UAUAAAGACAGCAAAUAUCCUCAUC-3') (*3*), which was consistent with the operation for downregulation of CK RNA. For the construction of stable PD-L1-positive 293FT cell lines, the 293FT cells were transfected with a lentiviral vector containing human PD-L1 gene (purchased from HanBio, Shanghai) for 24h, and then screened for the stable cell lines by adding Puromycin, following a standard protocol for stabilizing cell transfection (*4, 5*). Briefly, 10^5 293FT cells were seeded into 24-well plates. When the cell confluence reached 50%, the original medium was removed and 100 μL of medium containing lentiviral vector and polybrene (4 μg/mL) was added for infection of 8 h. The PD-L1 expression were regulated by controlling the dose of lentiviral vector (10^6 TU/mL for preparing PD-L1^{high} 293FT cells and 10^5 TU/mL for preparing PD-L1^{low} 293FT cells). Then, the transduction medium was replaced with fresh medium. After 24 hours, puromycin (2 μg/mL, A1113803, Gibco) was added to each well to screen the transduced 293FT cells.

Clinical blood samples. According to the National Comprehensive Cancer Network clinical practice guideline of NSCLC, surgical resection was directly conducted on most early-stage (clinical stage IA-IB) patients. Locally advanced patients (clinical stage IB-IIIB) were given 2 - 4 courses of neoadjuvant immunotherapy. Following clinical practice, radiologic response assessment was conducted after the second treatment course to determine if patients met the criteria for surgical resection or still need to continue with another treatment course. Locally advanced (clinical

unresecSI Appendix Table Stage IIIB) or advanced (clinical stage IV) NSCLC patients received neoadjuvant immunotherapy as first-line treatment. Before each treatment course or surgery, 5 mL blood samples were collected and separated by gradient centrifuge to obtain the peripheral blood mononuclear cells. Patient information is provided in **SI Appendix Table S3**. For patients receiving neoadjuvant therapy, radiographic response was assessed according to the Response Evaluation Criteria in Solid Tumors (RECIST) criteria 1.1 (*6*). After surgery, the resected primary tumor and lymph node tissues were assessed by a thoracic pathologist to assess the therapeutic effect. The whole resected lymph node received pathological examination. If the diameter of the residual tumor was less than 3 cm, the whole tumor was sectioned serially. For tumors larger than 3 cm, at least one slide per centimeter of the greatest tumor diameter would be reviewed for each specimen. Primary tumors were assessed for the percentage of residual viable tumor (RVT) on routine hematoxylin and eosin staining after operation. Tumors with no more than 10% RVT were considered as major pathological remission (MPR), and tumors without RVT were considered as pathologic complete response (pCR). The whole tumor tissue was re-checked if MPR or pCR was diagnosed.

Target mRNA identification by qPCR. RNA extraction was conducted using a kit (RC112-01, Vazyme) according to the instruction manual. 50 ng of template was used for gene amplification by a commercial kit (RR066A, Takara). Thermocycling conditions were: 42 °C for 5 min, 95 °C for 10 s, 40 cycles: 95 °C for 5 s, 60 °C for 34 s. The GAPDH gene was used as the reference gene. The value of ΔCt was calculated based on the following equation: ΔCt = Ct (Target RNA) – Ct (GAPDH RNA).

Western Blot. About 10^6 of cells were lysed in 100 μL of RIPA buffer (89901, Thermo Fisher Scientific), including 1 × protease inhibitor cocktail (P1005, Beyotime), on ice for 30 min. The cell lysates were centrifuged at 12000 rpm for 10 min. The obtained supernatant solutions were mixed with 5 × loading buffer (SL1189, Coolaber) and incubated at 95 °C for 10 min. Proteins were separated using 12% sodium dodecyl sulfate-polyacrylamide gel electrophoresis (100 V, 1.5 h) and transferred to polyvinylidene fluoride membranes (120 V, 2 h). Membranes were probed using primary antibodies against E-cadherin (1:2000; 60335-1-Ig, Proteintech), cytokeratins (1:1000; ab7753, Abcam), vimentin (1:1000; ab8978, Abcam), N-cadherin (1:1000; 11039-R020, Sino Biological), PD-L1 (1:1000; ab205921, Abcam), and β-actin (1:20000; 66009-1-Ig, Proteintech), respectively. After incubated with horseradish peroxidase-conjugated secondary antibody (Anti-mouse IgG-HRP, 1:10000, P03S01; Anti-rabbit IgG-HRP, 1:10000, P03S02; both from Gene-Protein Link), all membranes were developed using a chemiluminescence system (Minichemi TM, Sagecreation).

Immunofluorescence. The cells were incubated with 4% polyoxymethylene for 10 min and 0.1% Triton for 10 min. Between all following steps, cells were washed three times in PBS. The cells were incubated with 5% BSA for 30 min. For EMT identification, primary antibodies against E-cadherin (1:200; 60335-1-Ig, Proteintech), cytokeratins (1:100; ab7753, Abcam), vimentin (1:100; ab8978, Abcam), and N-cadherin (1:100; 11039-R020, Sino Biological) were mixed with the cells for 2 h at room temperature. For CTC identification, primary antibodies against CD45 (1:100, ab40763, Abcam) and CK (1:100; ab7753, Abcam) were mixed with the cells for 2 h at room temperature. The cells were incubated with Alexa Fluor 488-labeled or Alexa Fluor 647-labeled secondary antibody (Anti-mouse IgG, 1:1000, A-10680; Anti-rabbit IgG, 1:1000, A-11034; Anti-mouse IgG, 1:1000, A-31571, all from Thermo Fisher Scientific) for 1 h and nuclear dye DAPI for 10 min.

References

1. H. Guo, P. Li, L. Su, K. Wu, K. Huang, R. Lai, J. Xu, D. Sun, S. Li, Z. Deng, Y. Wang, H. Guo, Z. Chen, S. Wang, Low expression of IL-37 protein is correlated with high Oct4 protein expression in hepatocellular carcinoma. *Gene* **737**, 144445 (2020).
2. Y. Zou, Y. Zhen, Y. Zhao, H. Chen, R. Wang, W. Wang, P. Ma, D. Zhi, B. Ju, S. Zhang, pH-sensitive, tail-modified, ester-linked ionizable cationic lipids for gene delivery. *Biomater. Adv.* **139**, 212984 (2022).
3. G. Breton, B. Yassine-Diab, L. Cohn, M. R. Boulassel, J. P. Routy, R. P. Sékaly, R. M. Steinman, siRNA knockdown of PD-L1 and PD-L2 in monocyte-derived dendritic cells only modestly improves proliferative responses to Gag by CD8(+) T cells from HIV-1-infected individuals. *J. Clin. Immunol.* **29**, 637-645 (2009).

4. Q. Y. Zhang, X. D. Li, S. Q. Liu, C. L. Deng, B. Zhang, H. Q. Ye, Development of a stable Japanese encephalitis virus replicon cell line for antiviral screening. *Arch. Virol.* **162**, 3417-3423 (2017).
5. Q. Y. Hu, Y. Yuan, Y. C. Li, L. Y. Yang, X. Y. Zhou, D. Q. Xiong, Z. Y. Zhao, Programmed cell death ligand 1-transfected mouse bone marrow mesenchymal stem cells as targeted therapy for rheumatoid arthritis. *BioMed Res. Int.* **2021**, 5574282 (2021).
6. E. A. Eisenhauer, P. Therasse, J. Bogaerts, L. H. Schwartz, D. Sargent, R. Ford, J. Dancey, S. Arbuck, S. Gwyther, M. Mooney, L. Rubinstein, L. Shankar, L. Dodd, R. Kaplan, D. Lacombe, J. Verweij, New response evaluation criteria in solid tumours: revised RECIST guideline (version 1.1). *Eur. J. Cancer* **45**, 228-247 (2009).

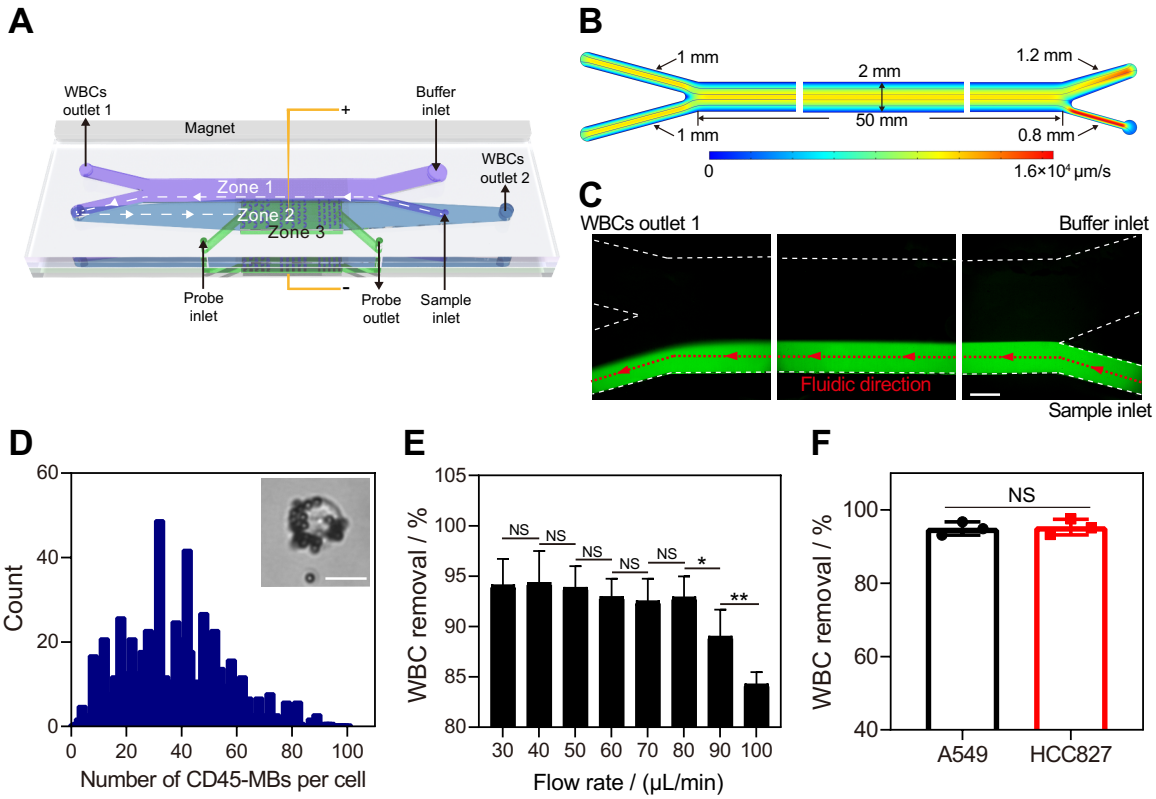

Fig. S1. Characterization of NICHE for WBC separation. (**A**) Schematic of the structure of NICHE. (**B**) Simulation of flow rate distribution in the channel of WBC-Removal Layer. (**C**) Laminar flow of sodium fluorescein (green) in the channel of the WBC-Removal Layer, identifying the flow path for CTCs, whilst WBCs are removed from the flow by a magnet at the top. Scale bar: 0.5 mm. Images are taken from inlet and outlet areas as well as the middle portion of the WBC-Removal Layer. (**D**) Distribution of the number of CD45-MBs bound to 1000 Jurkat T cells. The inset shows a Jurkat T cell labeled with multiple CD45-MBs. Scale bar: 10 μm. (**E**) Removal efficiency of Jurkat T cell (10^6 cells / mL) in the WBC-Removal Layer under different flow rates, from 30 μL/min to 100 μL/min. (**F**) The removal efficiency of Jurkat T cells (10^6 cells/mL) in the WBC-Removal Layer under the flow rate of 80 μL/min when mixed with two types of human lung cancer cells (A549 and HCC827, 100 cells/mL, 1 mL). *, *p-value* < 0.05. **, *p-value* < 0.01. NS, no significant difference. Error bars in (E) and (F) represent the standard deviation of three independent experiments.

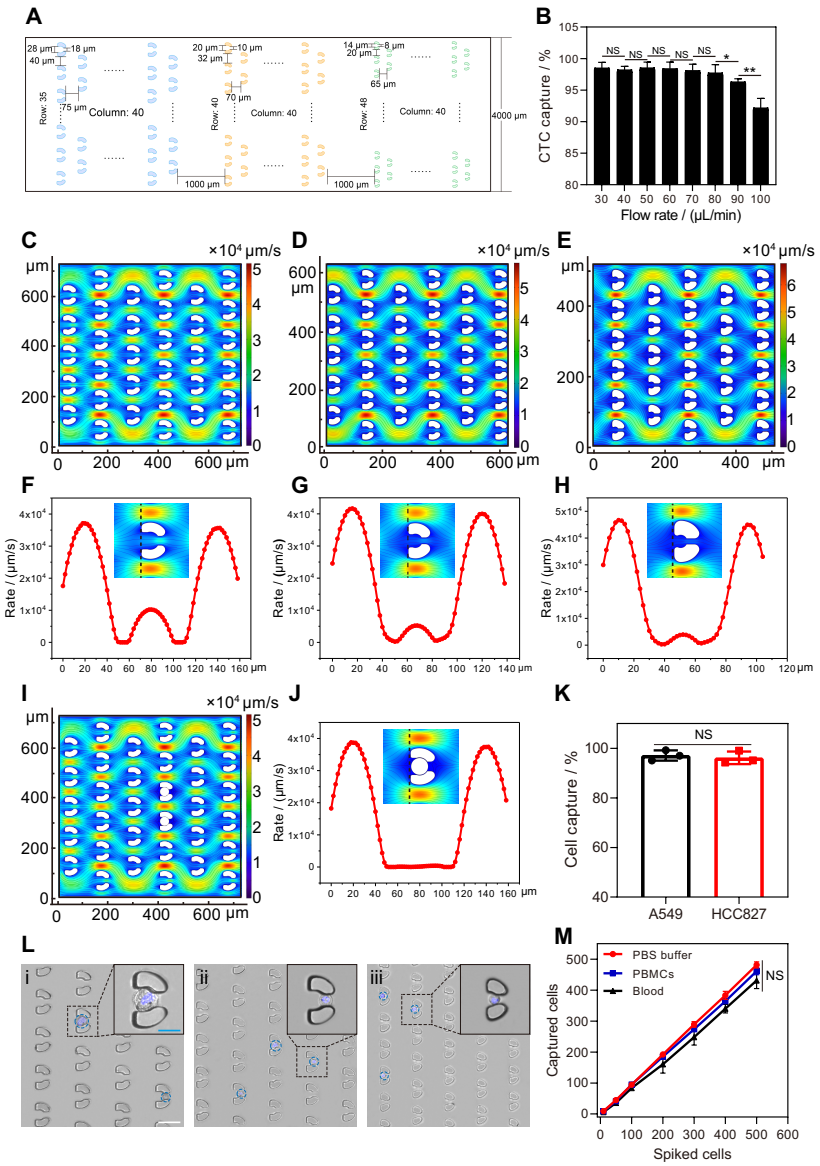

Fig. S2. Characterization of NICHE for CTC capture. (**A**) The layout and specification of microfluidic cell trap arrays in the CTC-Capture Layer. (**B**) Capture efficiency of A549 cells in the CTC-Capture Layer under different flow rates, from 30 μL/min to 100 μL/min. (**C**), (**D**), (**E**) and (**I**) Simulation of flow rate in part of the microfluidic cell trap array with large (C), middle (D), and small (E) sizes, and when two CTCs are trapped (I). (**F**), (**G**), (**H**) and (**J**) Simulation of flow rate distribution in a large (F), a middle (G) and a small (H) size of micro-traps, and when one CTC is trapped (J). The curves show the velocity change at the position of dotted line next to the micro-trap. (**K**) The capture efficiency of cancer cells (100 cells/mL, 1 mL) in the CTC-Capture Layer under the flow rate of 80 μL/min. (**L**) Three groups of microfluidic cell "bagatelle" trap arrays to capture CTCs (which are larger than WBCs): (i) 28 μm inlet and 18 μm outlet; (ii) 20 μm inlet and 10 μm outlet; and (iii) 14 μm inlet and 8 μm outlet. Blue fluorescence is from DAPI dye for identifying the cell nucleus. Scale bar (white): 50 μm. The insets show enlarged detail from the image (i), (ii), and (iii). Scale bar (blue): 25 μm. (**M**) The number of A549 cells recovered from the blood-mimetic samples captured by NICHE. A549 cells were spiked in 1 mL of buffer, 10^6 PBMCs, or 1 mL blood. Blood samples were first centrifuged by density gradient to obtain PBMCs, and then separated by the chip. Cells in the buffer and in PBMCs were separated directly on the chip. *, *p-value* < 0.05. **, *p-value* < 0.01. NS, no significant difference. Error bars in (B), (K) and (M) represent the standard deviation of three independent experiments.

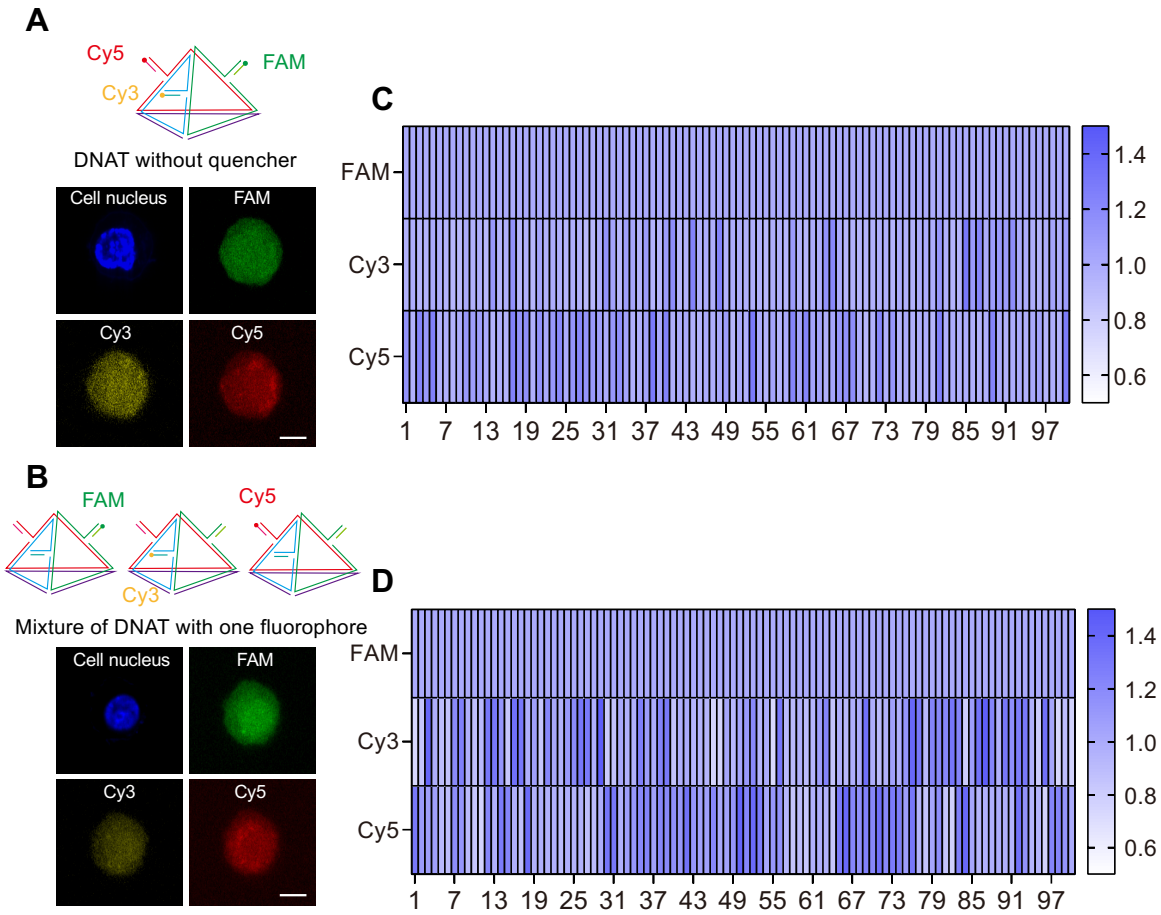

Fig. S3. Evaluation of uniformity between different detection channel after delivery. (**A**) and (**B**) Fluorescence images of cells after delivery of DNAT without quencher labels (A) or the mixture of three types of DNAT labeled with one fluorophore (B). Scale bar, 10 μm. (**C**) and (**D**) Ratio of fluorescence intensity of Cy3 channel or Cy5 channel to that of FAM channel. (C) The cells were incubated with DNAT without quencher labels. (D) The cells were incubated with the mixture of three types of DNAT labeled with a fluorophore. The total concentration of DNAT was 1 μM. 100 cells are counted in Figure (C) and (D).

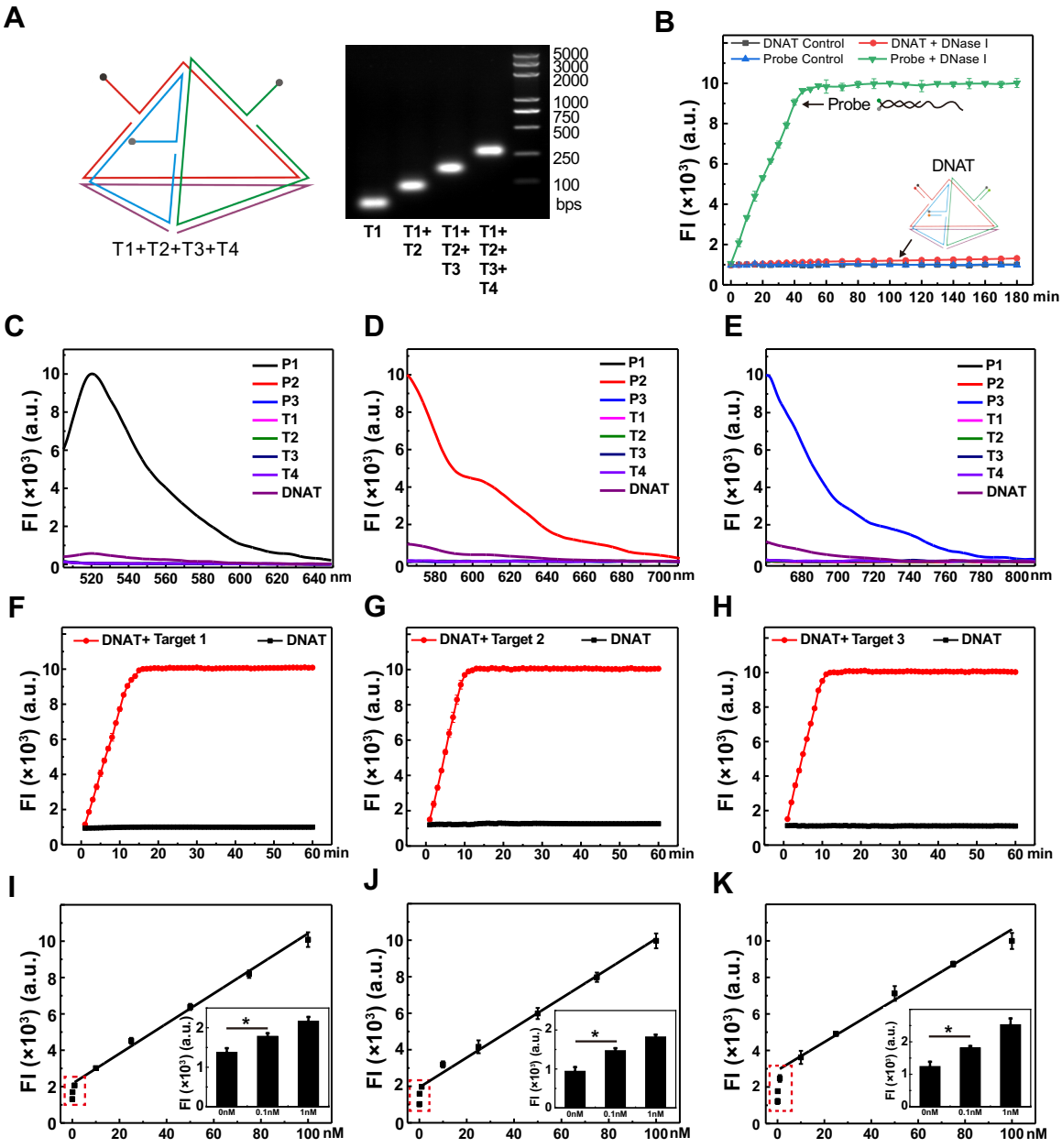

Fig. S4. Detection performance of DNAT probe in solution. (**A**) Agarose gel electrophoretic image of the structural assembly of DNAT probes. (**B**) Comparison of the ability of tetrahedral structured probes to resist enzymatic degradation with that of conventional probes. Conventional probe is assembled by sequences T1 and P1. DNase I, 1 U/mL. (**C**), (**D**) and (**E**) Fluorescent characterization of each component sequence of DNAT probe and the assembled DNAT probe in FAM channel (C), Cy3 channel (D) and Cy5 channel (E). FI, fluorescent intensity. (**F**), (**G**) and (**H**) Response time of the DNAT probe for detecting 100 nM of GAPDH RNA (F), PD-L1 RNA (G) and CK RNA (H). (**I**), (**J**) and (**K**) Calibration curves of the DNAT probe for the detection of GAPDH RNA (I), PD-L1 RNA (J) and CK RNA (K). Inset: the fluorescent intensity of DNAT probe for detecting 0.1 nM and 1 nM of target RNA, and a blank control group (without adding target RNA). The concentration of DNAT probe was 1 μM. *, *p-value* < 0.05. Error bars in (B) and (F)-(K) represent the standard deviation of three independent experiments.

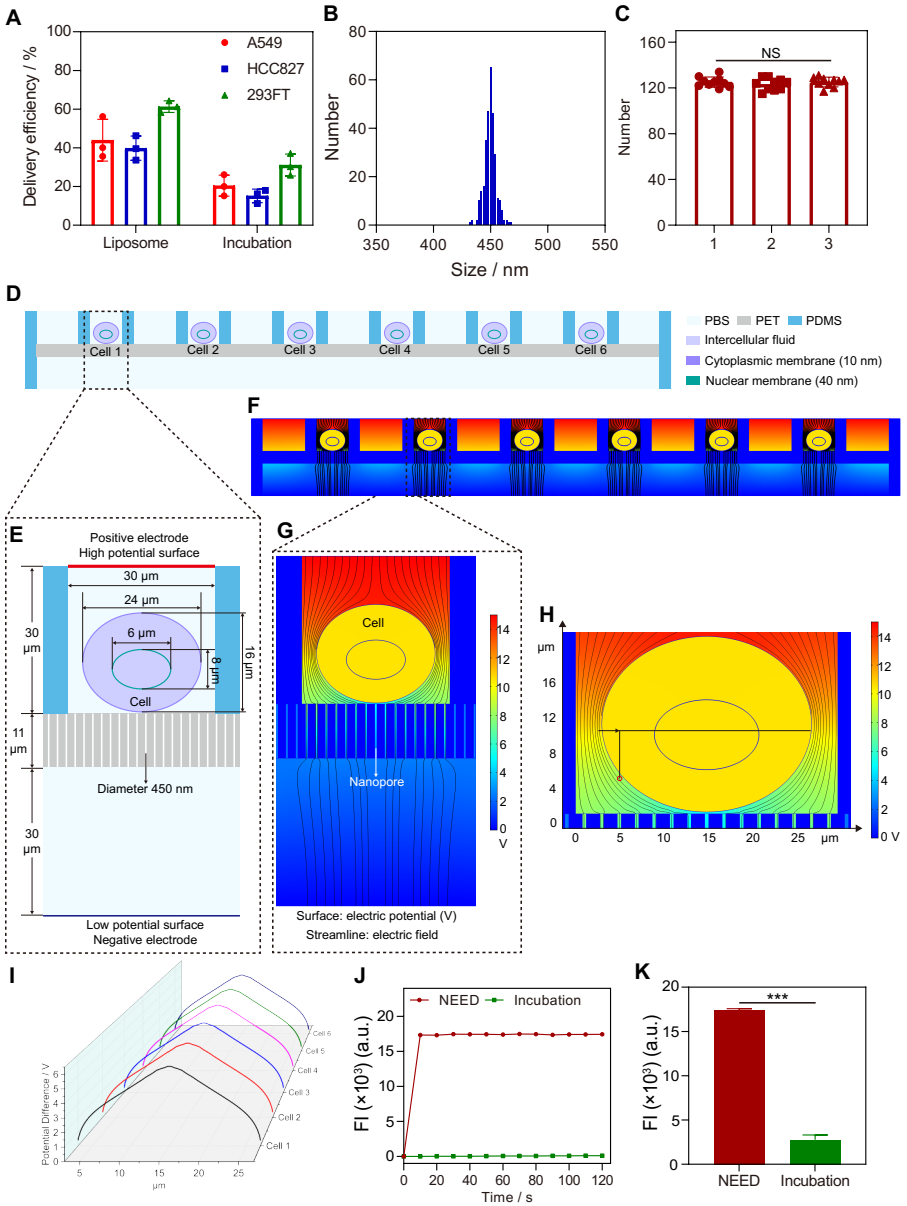

Fig. S5. Delivery ability of NEED. (**A**) Delivery efficiency of DNAT probes in HCC827, A549, and 293FT cells by liposome-based delivery and simple incubation with a free probe. The statistical data are obtained by counting 1000 cells/chip from three independent assays. (**B**) Pore size distribution of nanopores on the nanomembrane. (**C**) The number of nanopores on a 10 μm × 10 μm nanomembrane. Statistics were counted 10 times on each of the three membranes (1, 2, and 3) separately. (**D**) Prototype of simplified NEED device used to simulate the electric potential using the multiphysics simulation package, COMSOL Multiphysics 5.5. PBS, phosphate buffer saline. PET, polyethylene terephthalate. PDMS, polydimethylsiloxane. (**E**) Enlarged view of a cell in Figure (D). (**F**) Distribution of electric potential around the cells. (**G**) Enlarged view of the electrical potential distribution around a cell in Figure (F). (**H**) Enlarged view of the electrical potential distribution around the cell in Figure (G). (**I**) The electrical potential difference between the inside and outside of the cell membrane measured at the circle every 0.1 μm along the direction of the arrow in Figure (H). (**J**) Fluorescence intensity detected in A549 cells after delivery with Cy5-labeled DNAT probes (without labeling quencher) by NEED and by incubation. (**K**) Fluorescence intensity detected in 100 A549 cells after 1 hour of delivery with Cy5-labeled DNAT probes (without labeling quencher) by NEED and by incubation. NS, no significant difference. ***, *p-value* < 0.001. Error bars in (J) and (K) represent the standard deviation of three independent experiments.

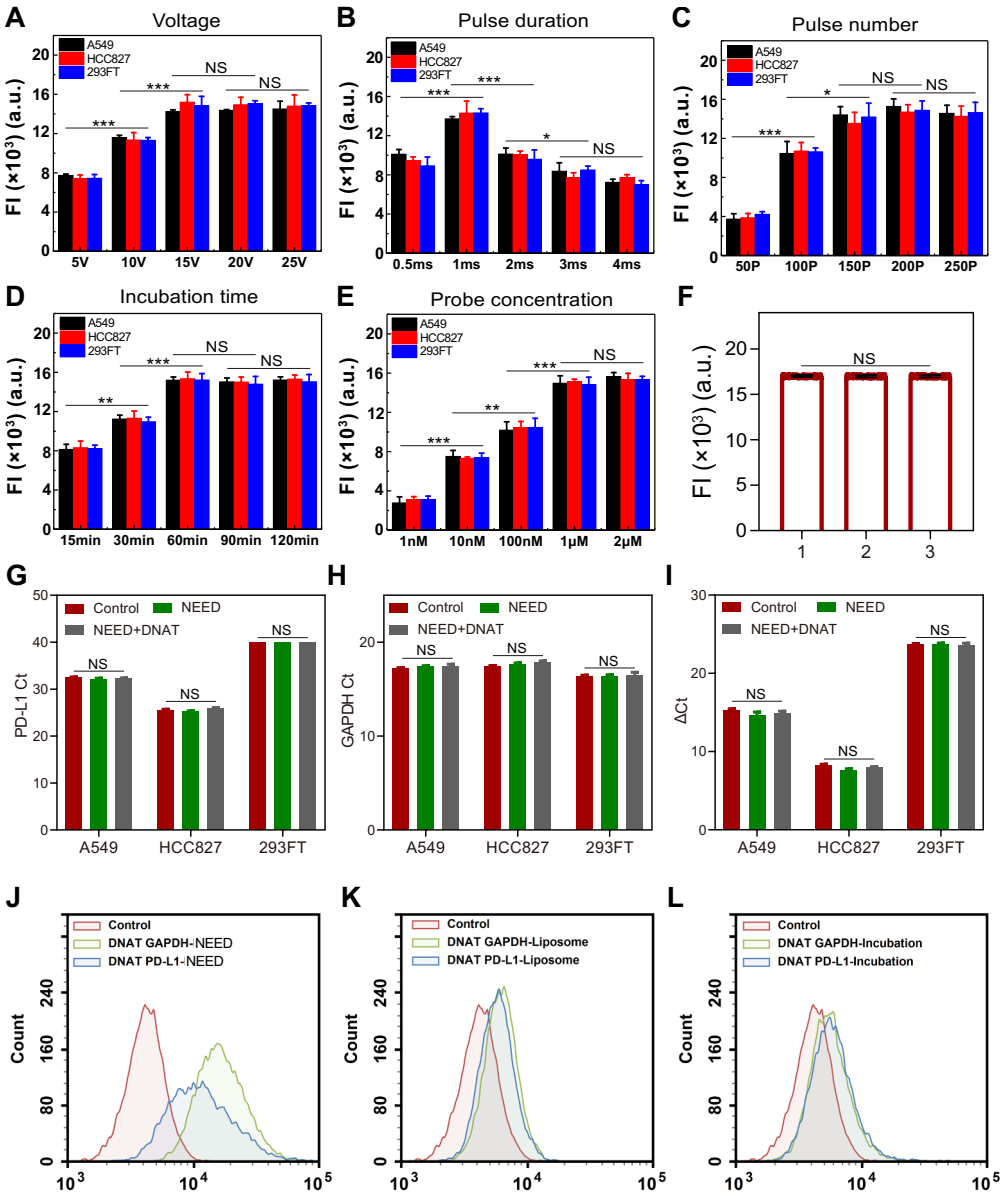

Fig. S6. Condition optimization of probe delivery and DNAT probe detection. (**A**), (**B**) and (**C**) The fluorescence intensity of FAM-labeled DNAT probes (without labeling quencher) in cells under different electroporation voltages (A), pulse duration (B), and pulse number (C). (**D**) Optimization of incubation time after delivering DNAT probe into cells. (**E**) Optimization of the concentration of DNAT probe delivered into cells. FI, the fluorescence intensity of FAM channel. (**F**) Fluorescence intensity detected in 100 A549 cells after 1 hour of delivery with DNAT probes (without labeling quencher) by NEED and by incubation. 1, 2, and 3 represent three independent experiments. (**G**) The Ct value of PD-L1 detected by qPCR. Control, cells without any treatment. NEED, cells treated with NEED yet without delivering DNAT probes. NEED+DNAT, cells delivered with DNAT probes by NEED. 293FT cell did not express PD-L1 RNA, and its Ct value of PD-L1 was set at 40. (**H**) The Ct value of GAPDH detected by qPCR. (**I**) The Ct difference between the Ct value of PD-L1 RNA and the Ct value of GAPDH RNA. The value of ΔCt is negatively correlated with the concentration of target RNA. (**J**), (**K**) and (**L**) Flow cytometry analysis of fluorescence intensity after delivering DNAT probe in HCC827 cells by NEED (J), liposome-based delivery (K) and simple incubation with free probe (L). *, *p-value* < 0.05. **, *p-value* < 0.01. ***, *p-value* < 0.001. NS, no significant difference. Error bars in (A)-(E) and (G)-(I) represent the standard deviation of three independent experiments.

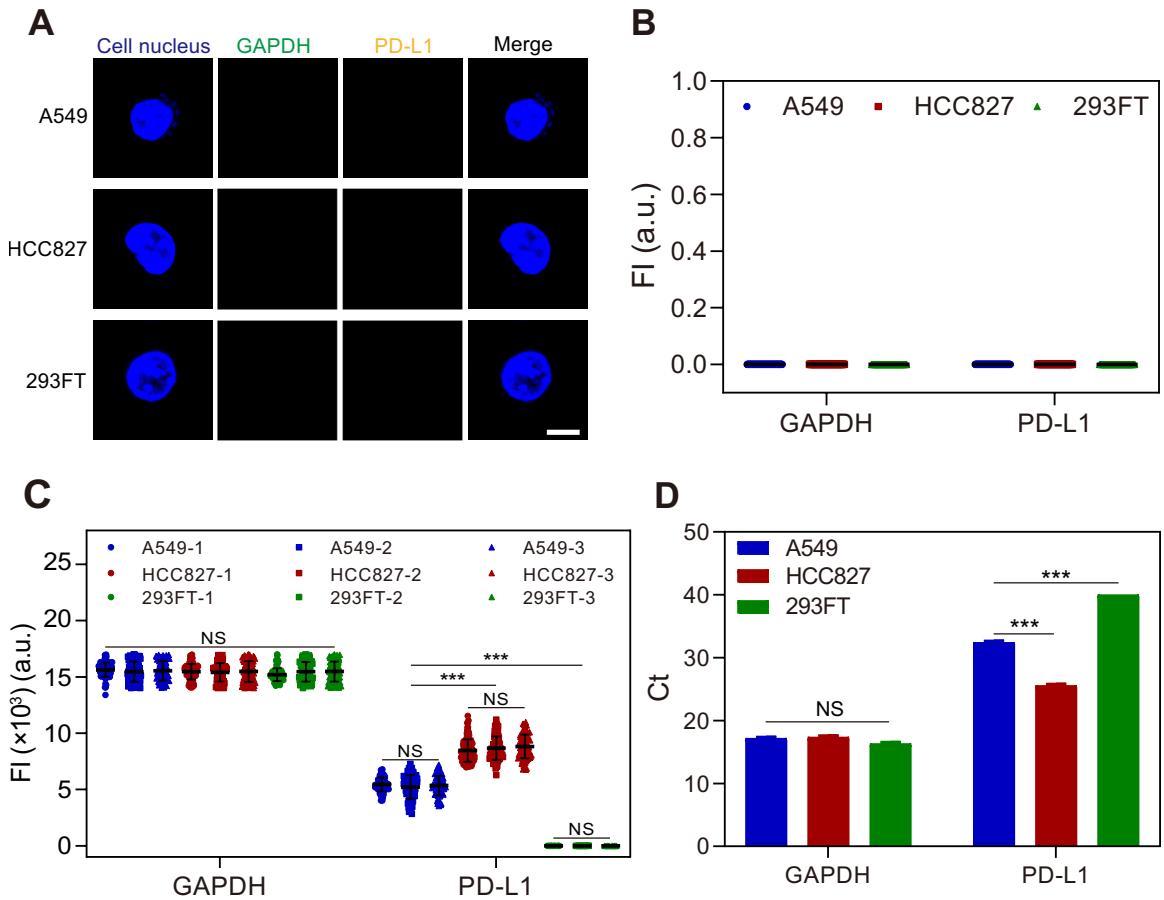

Fig. S7. Relative quantification of target mRNA in cells. (**A**) Fluorescence images of cells without DNAT probe delivery. Scale bar, 10 μm. (**B**) Average fluorescent intensity of 100 cells without DNAT probe delivery. (**C**) Cell fluorescence intensity after delivery of DNAT probes by NICHE. Error bars represent the standard deviation of 100 cells. 1, 2, and 3 represented the three individual tests, respectively. (**D**) Results of qPCR for analysis of the GAPDH mRNA and PD-L1 mRNA in cells. ***, *p-value* < 0.001. NS, no significant difference. Error bars in (D) represent the standard deviation of three independent tests.

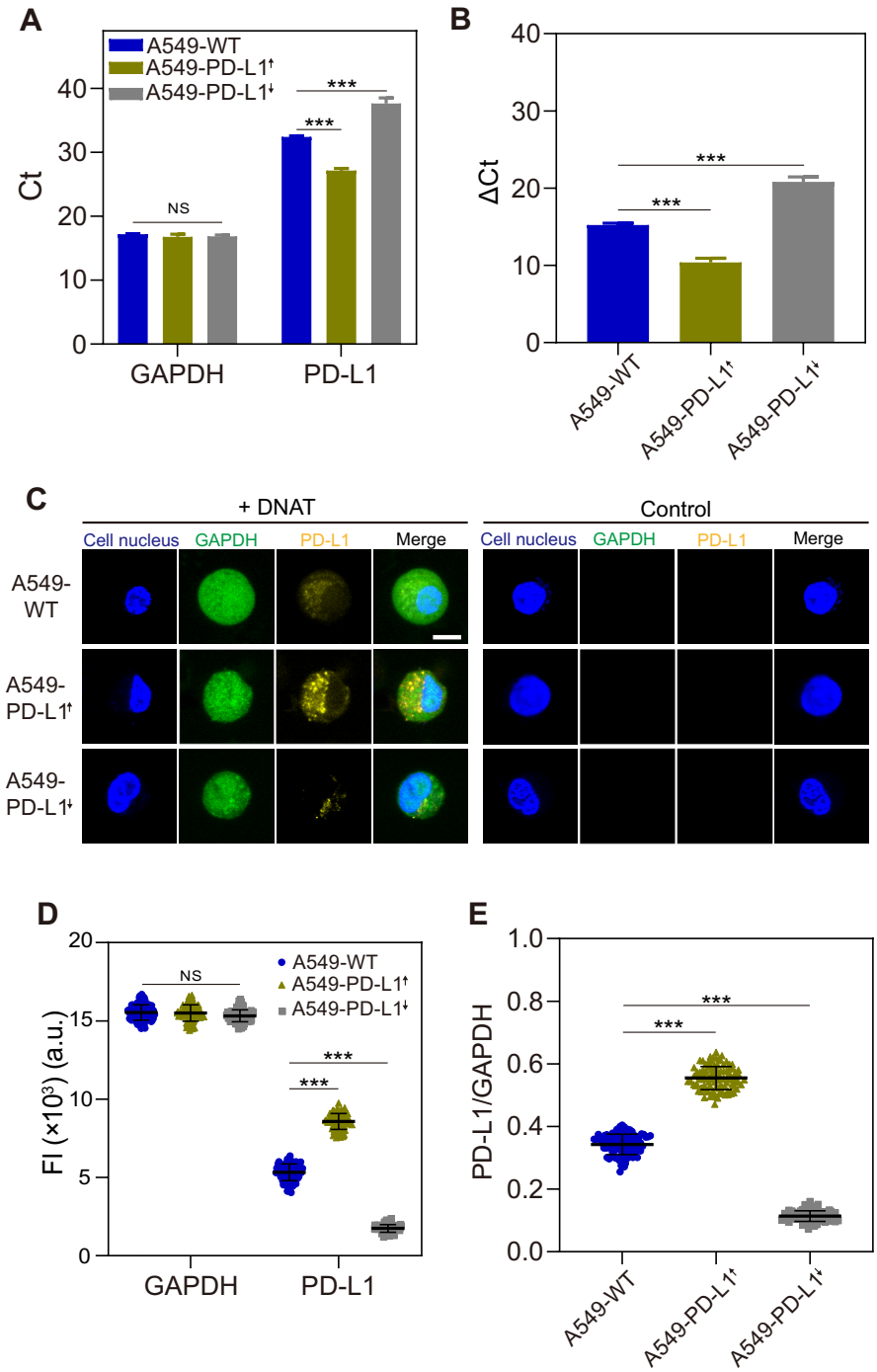

Fig. S8. Specific validation of DNAT probe for detecting PD-L1 in living cells. (**A**) Relative quantification of target mRNA by qPCR. A549 - WT, wild type A549 cells. A549 - PD-L1$^{\uparrow}$, PD-L1-overexpressed A549 cells. A549 - PD-L1$^{\downarrow}$, the expression of PD-L1 in A549 cells is down-regulated by siRNA. (**B**) The difference between the Ct value of PD-L1 RNA and the Ct value of GAPDH RNA. The value of ΔCt is negatively correlated with the concentration of target RNA. (**C**) Fluorescent images of cells detected by DNAT probes. + DNAT, cells delivered with DNAT probe. Control, cells without delivery of DNAT probe. Scale bar, 10 μm. (**D**) Cell fluorescence intensity after delivery of DNAT probes by NICHE. Error bars represent the standard deviation of 300 cells from three independent experiments. (**E**) Ratios of fluorescent intensity from 300 cells. ***, *p-value* < 0.001. NS, no significant difference. Error bars in (A) and (B) represent the standard deviation of three independent tests.

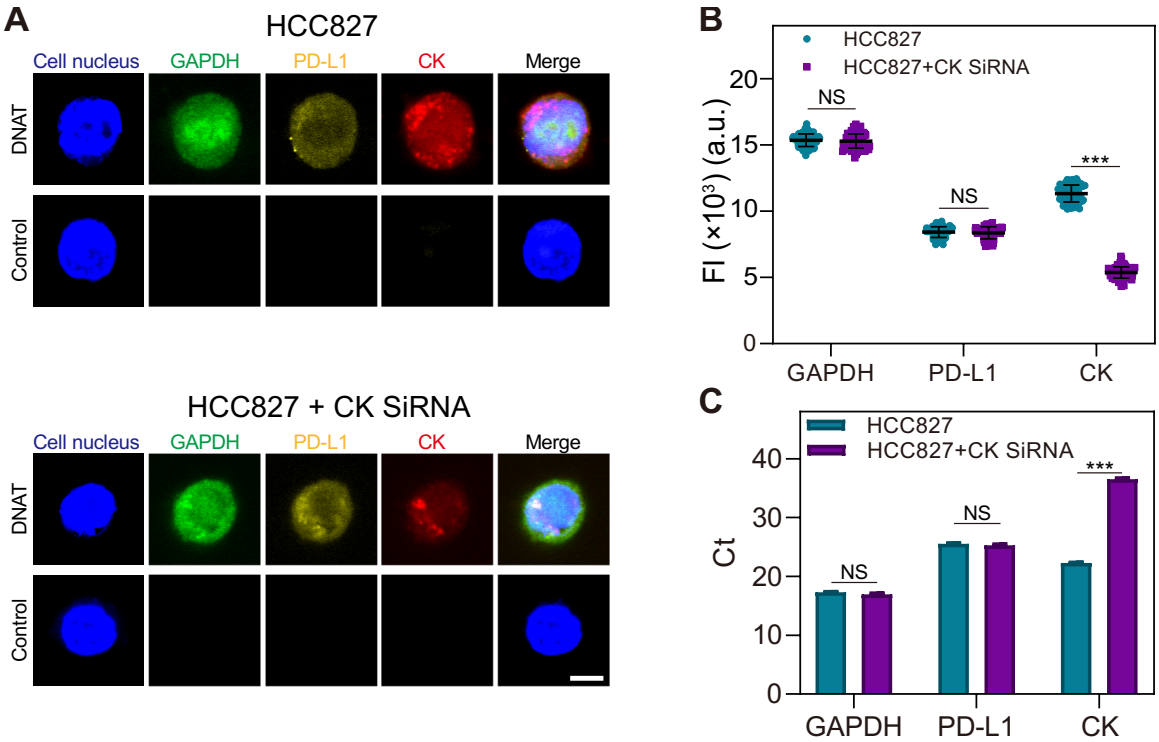

Fig. S9. Specific validation of DNAT probe for detecting CK in living cells. (**A**) Multiple target RNA detection in HCC827 cells by DNAT probe. HCC827 + CK siRNA, the expression of CK in HCC827 cells is down-regulated by siRNA. Scale bar, 10 μm. (**B**) Fluorescence intensity of individual cells detected by NICHE. Error bars represent the standard deviation of 100 cells. (**C**) Relative quantification of target mRNA by qPCR. ***, *p-value* < 0.001. NS, no significant difference. Error bars in (C) represent the standard deviation of three independent tests.

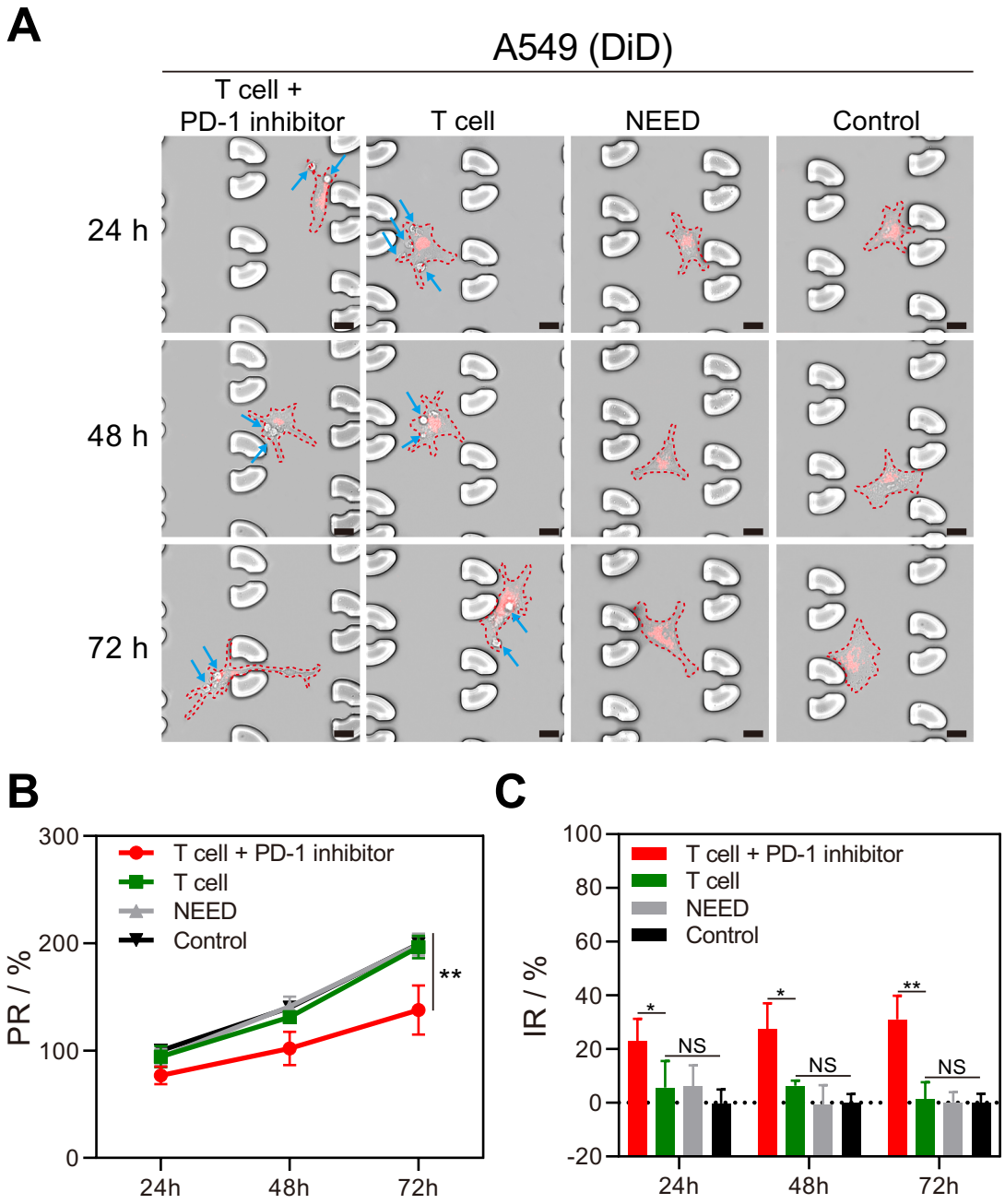

Fig. S10. Co-culture of A549 cells with immune T cells and PD-1 inhibitor. (**A**) Time-lapse images of co-cultured cells in a single Regions of Interest (ROI). T cell + PD-1 inhibitor, cells were co-cultured with Jurkat T cells and PD-1 inhibitor. T cell, cells were co-cultured with Jurkat T cells. Control, the cells without co-culture with Jurkat T cells. A549 cells were stained with DiD dye (Red) for long-term tracking. The blue arrows indicate Jurkat T cells. Scale bar: 20 μm. (**B**) The proliferation rate (PR) of A549 cells in co-culture with Jurkat T cells. (**C**) The inhibition rate (IR) of A549 cells in co-culture with Jurkat T cells. *, *p-value* < 0.05. ***, *p-value* < 0.001. Error bars in (B), (C) represent the standard deviation of three independent experiments.

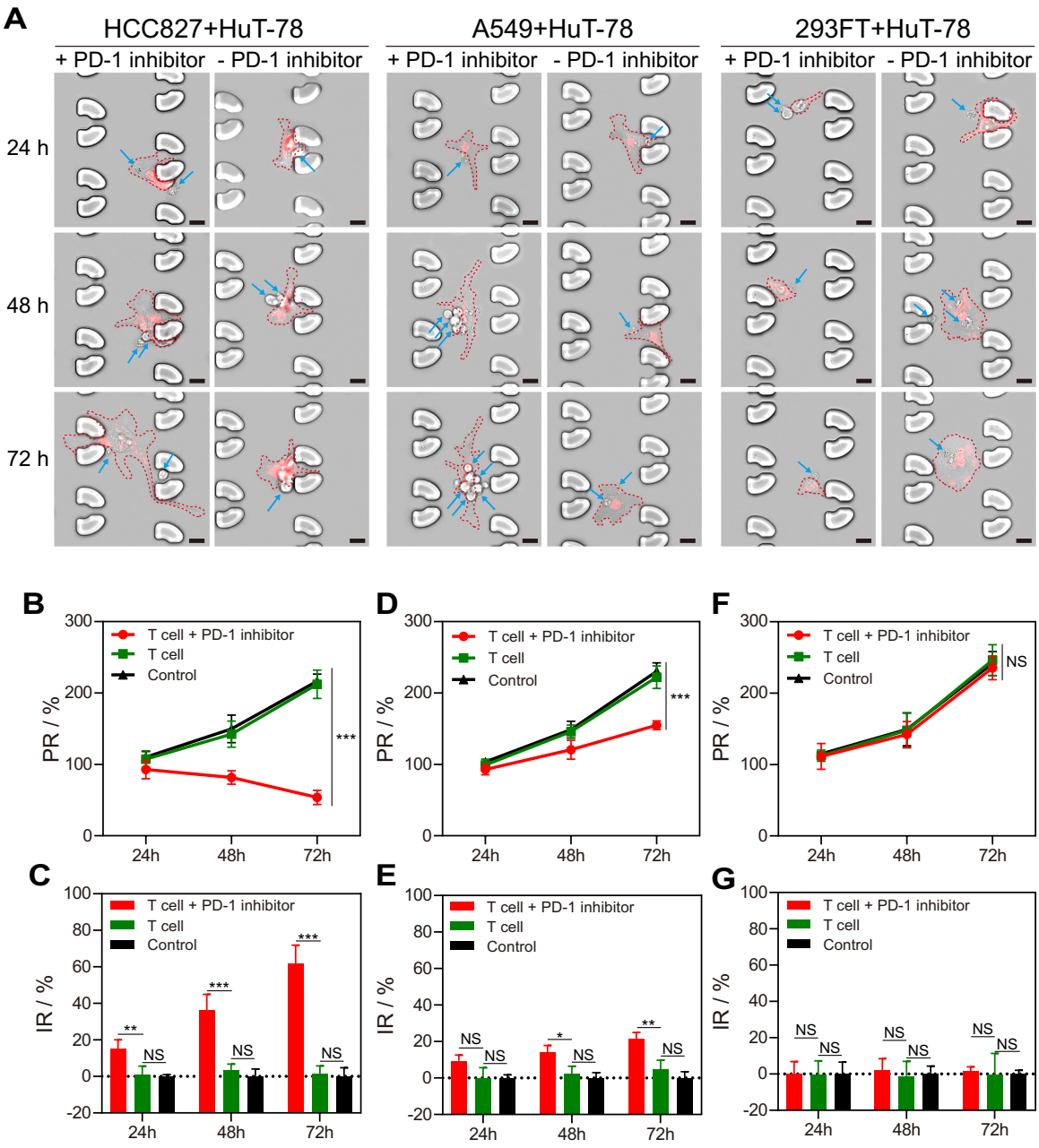

Fig. S11. Co-culture of tumor cells with HuT-78 cells. (**A**) Time-lapse images of co-cultured cells in a single ROI. + PD-1 inhibitor, cells were co-cultured with HuT-78 cells and PD-1 inhibitor. - PD-1 inhibitor, cells were only co-cultured with HuT-78 cells. HCC827 cells, A549 cells and 293FT cells are stained with DiD dye (Red) for long-term tracking. The blue arrows indicate Jurkat T cells. Scale bar: 20 μm. (**B**) - (**C**) The proliferation rate (PR) (B) and inhibition rate (IR) (C) of HCC827 cells. T cell + PD-1 inhibitor, cells were co-cultured with HuT-78 cells and PD-1 inhibitor. T cell, cells were co-cultured with HuT-78 cells. Control, the cells without co-culture with HuT-78 cells. (**D**) - (**E**) The proliferation rate (PR) (D) and inhibition rate (IR) (E) of A549 cells. (**F**) - (**G**) The proliferation rate (PR) (F) and inhibition rate (IR) (G) of 293FT cells. *, *p-value* < 0.05. **, *p-value* < 0.01. ***, *p-value* < 0.001. NS, no significant difference. Error bars in (B) - (G) represent the standard deviation of three independent experiments.

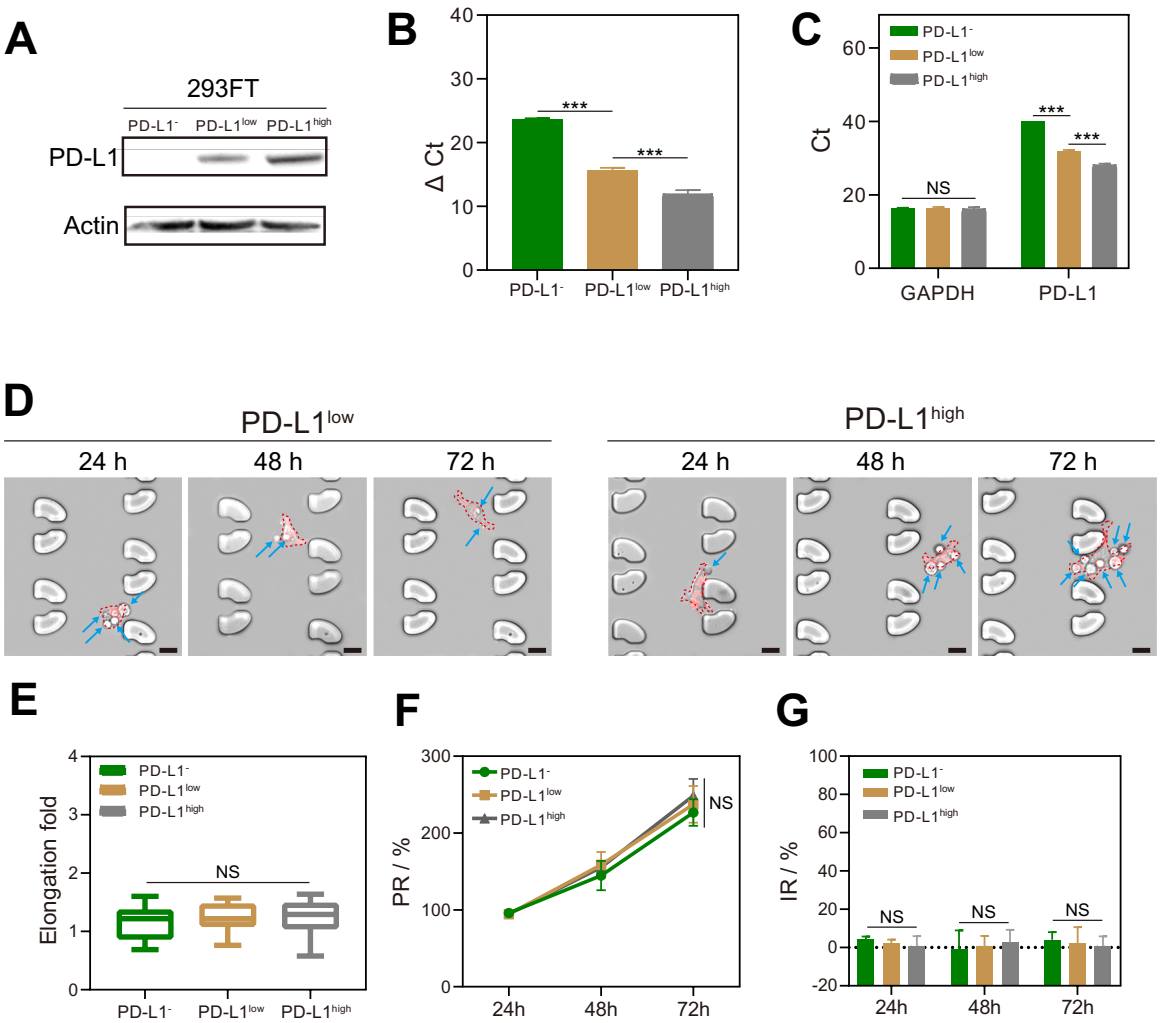

Fig. S12. Validation of immune response results by regulation of PD-L1. (**A**) PD-L1 protein expression identification by Western Blot. PD-L1^{low}, 293FT cells with a low copy of ectopic PD-L1. PD-L1^{high}, 293FT cells with a high copy of ectopic PD-L1. PD-L1^{-}, wild type 293FT cells. (**B**) Relative quantification of RNAs detected by qPCR. ΔCt is the difference between the Ct value of PD-L1 RNA and the Ct value of GAPDH RNA. The value of ΔCt is negatively correlated with the concentration of target RNA. PD-L1 is not expressed in 293FT cells, and the Ct value of PD-L1 is set at 40. (**C**) Results of qPCR for analysis of the GAPDH mRNA and PD-L1 mRNA in cells. (**D**) Confocal images of co-cultured cells. The cells are stained with DiD dye (Red) for long-term tracking. The blue arrows indicate Jurkat T cells. Scale bar: 20 μm. (**E**) Fold of morphological elongation after co-culture with Jurkat T cells (blocked with anti-PD-1 antibodies) for 72 hours. 300 cells are counted in each experiment. (**F**) The proliferation rate (PR) of 293FT cells and the PD-L1 overexpressed cells after incubation with Jurkat T cells and PD-1 inhibitor. (**G**) The inhibition rate (IR) of 293FT cells and the PD-L1 overexpressed cells after incubation with Jurkat T cells and PD-1 inhibitor. ***, *p-value* < 0.001. NS, no significant difference. Error bars in (B), (C) and (E) - (G) represent the standard deviation of three independent experiments.

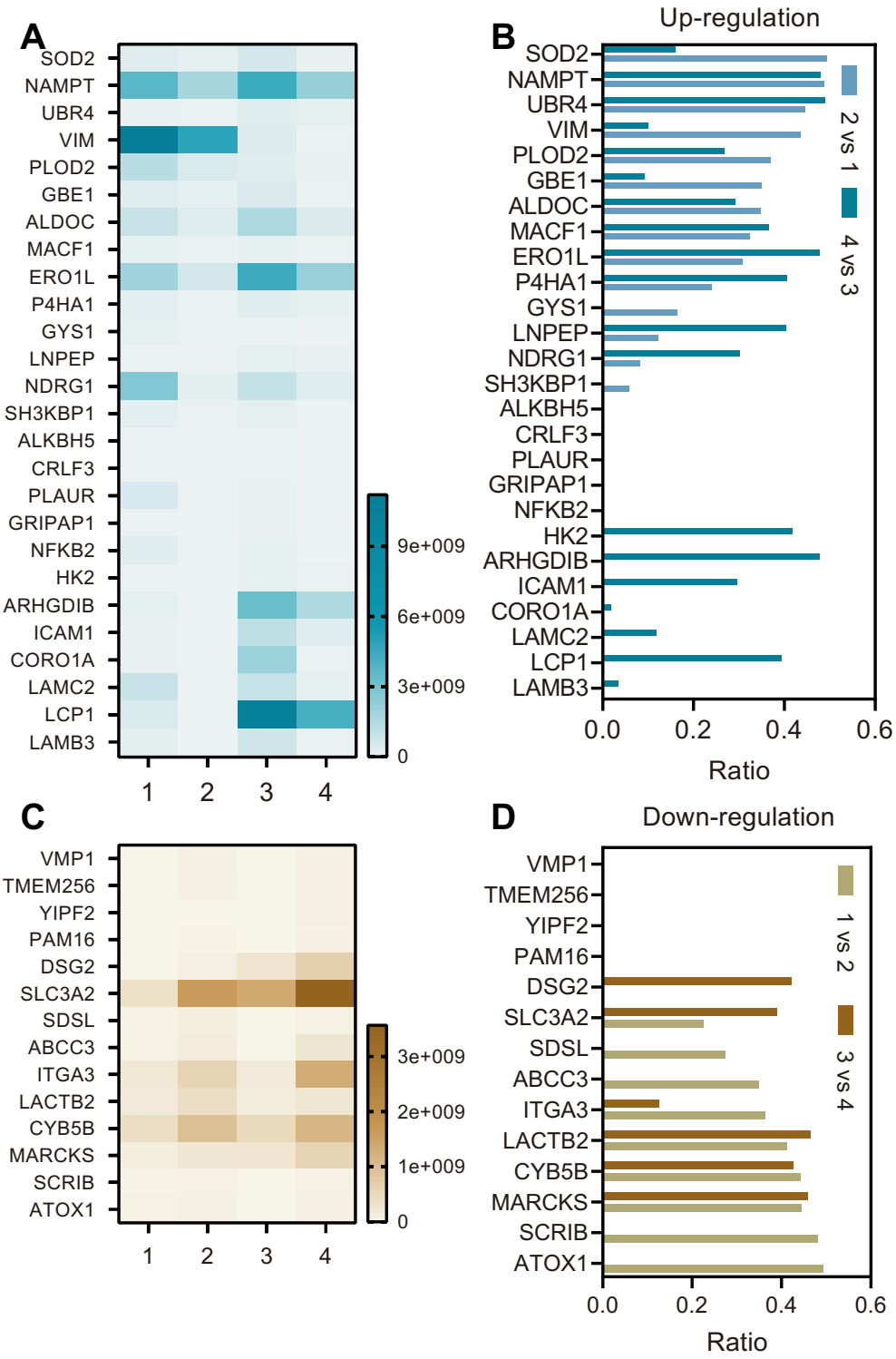

Fig. S13. Identification of potential regulatory proteins by label-free protein mass spectrometry. (**A**) Intensity of 26 up-regulated proteins in both A549 cells (PD-L1^{low} cells) and HCC827 cells (PD-L1^{high} cells) with morphological elongation. 1, A549 cells + Jurkat T cells + inhibitor; 2, A549 cells; 3, HCC827 cells + Jurkat T cells + inhibitor; 4, HCC827 cells. (**B**) The intensity ratio of 26 up-regulated proteins. (**C**) Intensity of 14 down-regulated proteins in both A549 cells (PD-L1^{low} cells) and HCC827 cells (PD-L1^{high} cells) with morphological elongation. (**D**) The intensity ratio of 14 down-regulated proteins.

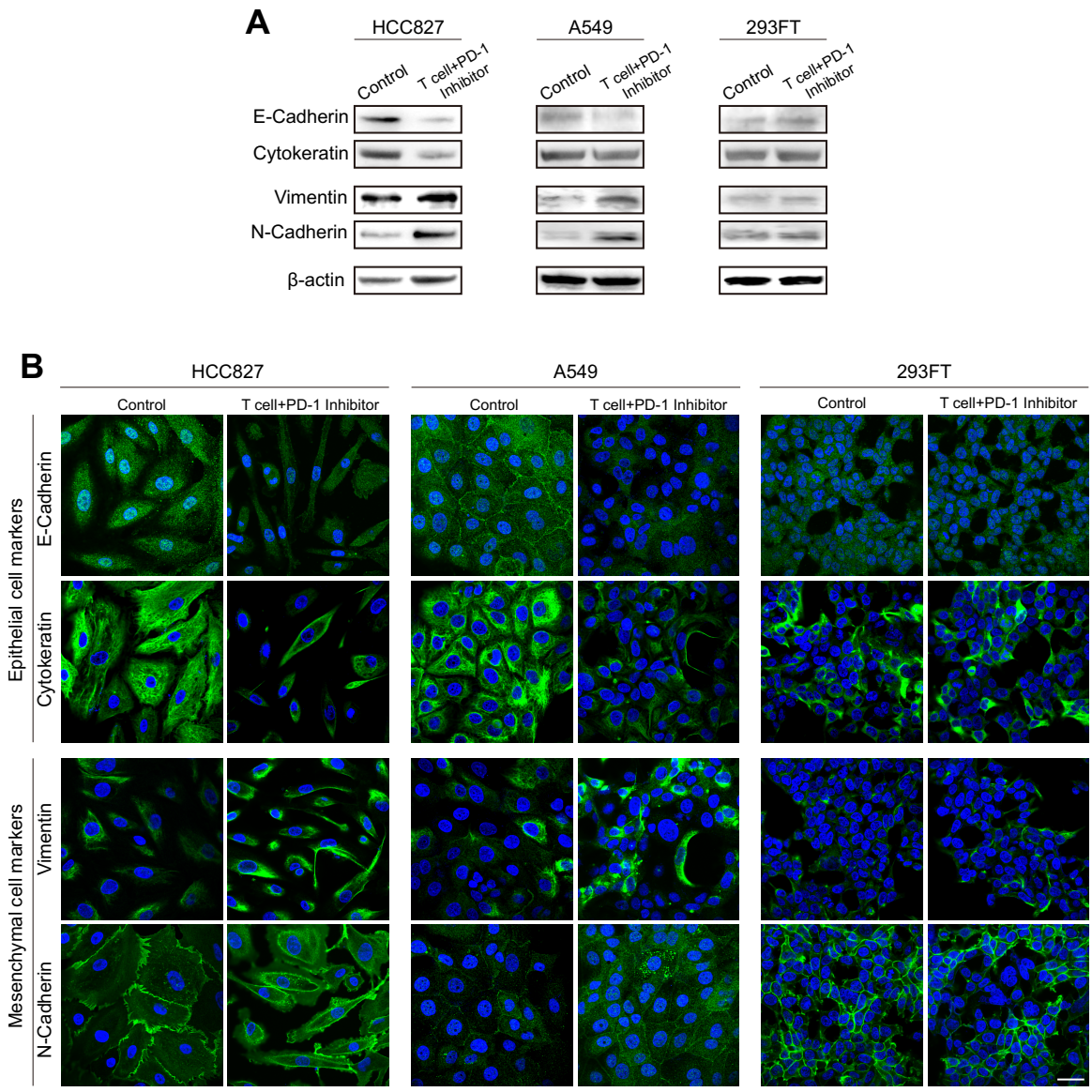

Fig. S14. Identification of epithelial-mesenchymal transition (EMT). (**A**) Protein expression identification by Western Blot to compare the change of EMT markers. Epithelial cell markers, E-cadherin and cytokeratin. Mesenchymal cell makers, vimentin and N-cadherin. β-actin is used as the house-keeping protein. (**B**) Immunofluorescence identification of cellular markers. Epithelial cell markers, E-cadherin and cytokeratin (green). Mesenchymal cell makers, vimentin and N-cadherin (green). DAPI is used to identify cell nucleus (blue). Scale bar: 25 μm.

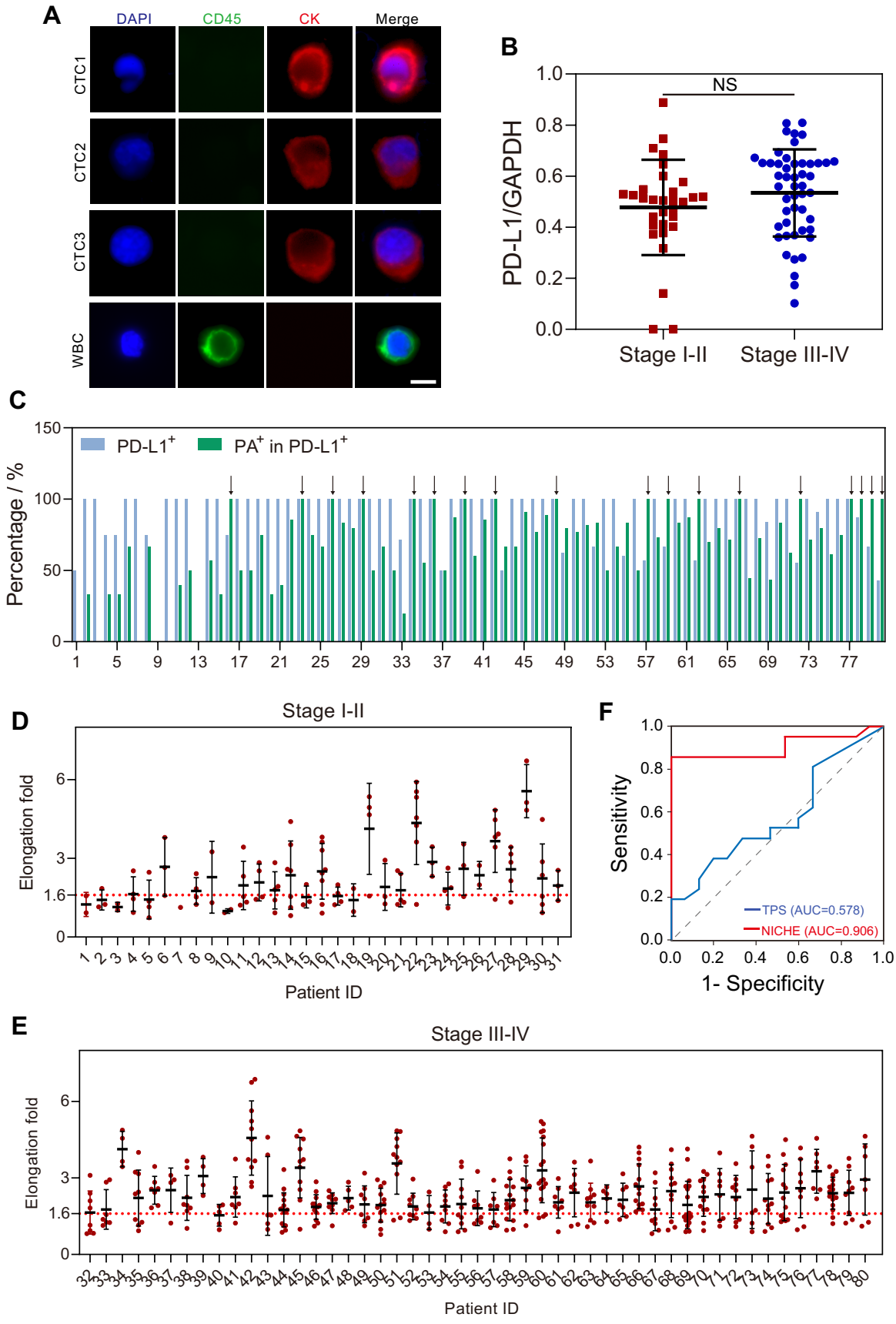
A
DAPI
CD45
CK
Merge
CTC1
CTC2
CTC3
WBC
B
NS
PD-L1/GAPDH
Stage I-II
Stage III-IV
C
PD-L1+
PA+ in PD-L1+
Percentage / %
D
Stage I-II
Elongation fold
Patient ID
F
Sensitivity
1- Specificity
TPS (AUC=0.578)
NICHE (AUC=0.906)
E
Stage III-IV
Elongation fold
Patient ID

Fig. S15. Detection in clinical blood samples from NSCLC patients. (**A**) Immunofluorescence staining for CTC identification. The CTCs were captured from patient NO. 57. Scale bar: 10 μm. (**B**) Weak correlation of PD-L1 expression in CTCs with cancer stages. Each plot represents the mean of PD-L1 expression in all CTCs from each patient. PD-L1/GAPDH, ratio of the fluorescent intensity of PD-L1 (Cy3 channel) and GAPDH (FAM channel). NS, no significant difference. (**C**) Percentage of $PD\text{-}L1^+$ CTCs in patient blood samples and PA^+ CTCs in all $PD\text{-}L1^+$ CTCs. The black arrows indicate 18 of the clinical samples that the PD-L1-positive CTCs all underwent distinct phenotype alteration with the introduction of T cells. (**D**) - (**E**) Elongation fold of individual CTCs obtained from 80 NSCLC patients. Each point represents a CTC. (D) The samples with stage I-II cancer. (E) The samples with stage II-IV cancer. (**F**) The receiver operating characteristic (ROC) plot analysis of NICHE and TPS in predicting immunotherapy efficacy. AUC, area under the curve.

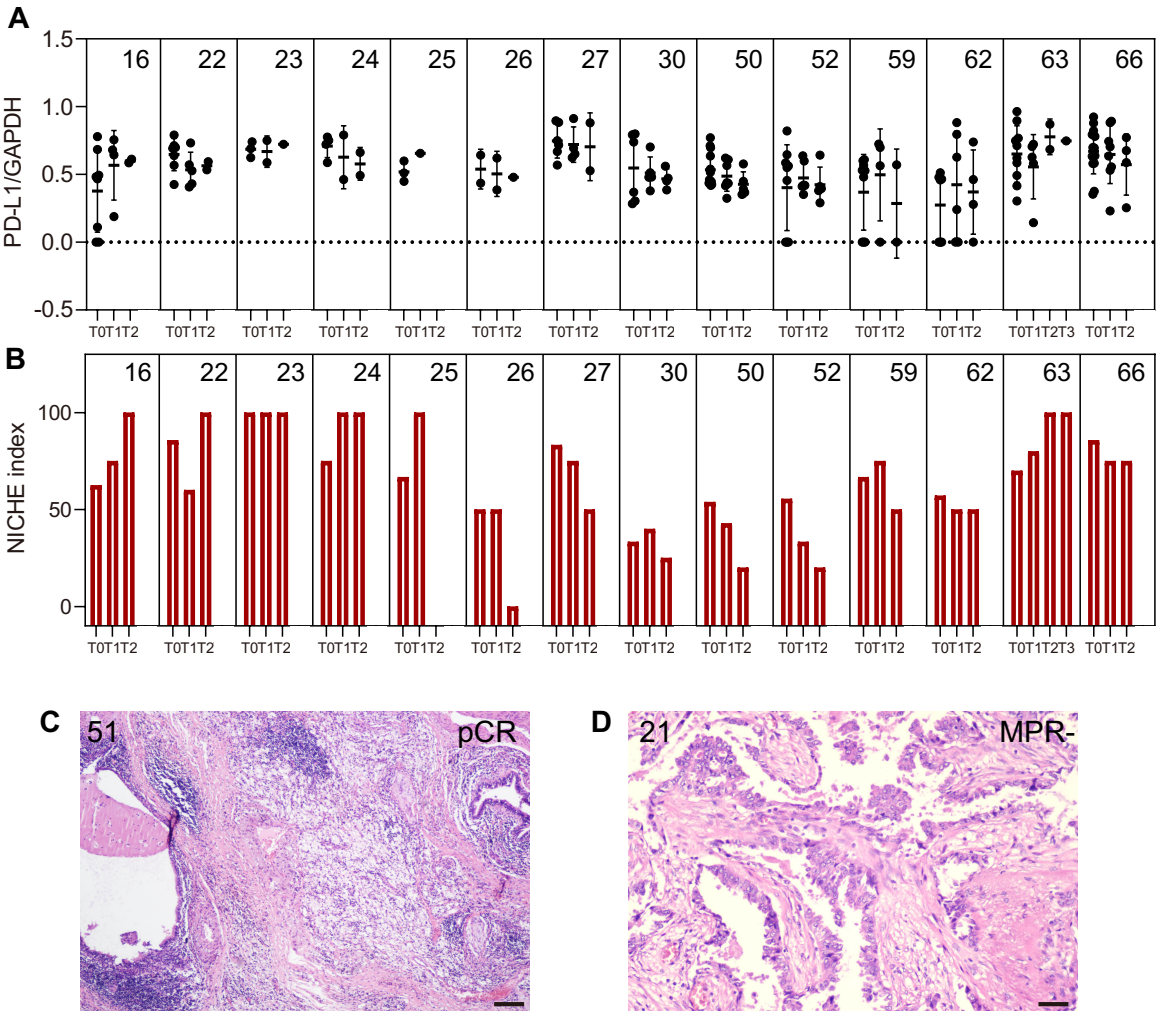

Fig. S16. NICHE for monitoring NSCLC patients throughout drug treatment periods. (**A**) Ratios of the fluorescent intensity of PD-L1 (Cy3 channel) and GAPDH (FAM channel) from each CTCs isolated from 5 mL blood samples of patients. (**B**) NICHE index for monitoring NSCLC patients. (**C**) and (**D**) Pathological section staining results of tumor tissues from patient NO. 51 (C) and patient NO. 21 (D). Scale bar: 200 μm (C); 50 μm (D).

Table S1. Sequences of DNAT probes and PCR primers.

Name	Sequence (5' to 3')
T1-GAPDH	BHQ-1- TGTTGCTGTAGCCAAATTCGTTCAGACCGAATCCCACGTAGTGTCGT ATAAACTGCCTGGCACATAGATACGTGCAATGA
T2-PD-L1	BHQ-1- AATGTGTATCACTTTGCTTCTGTAGCAAGCTCGGTCTGAATCATTGC ACGGTATTGGACCCTCGCATCTCCCTAGCGAGT
T3-CK	BHQ-2- GCTCAAACCACCCGCATAGCTACGTGGGATGCTTGCTACAACTCGC TAGGTTACAACGATTGGCTCTGTCTATACGACAC
T4	TATCTATGTGCCAGGCAGTTGACAGAGCCAATCGTTGTAAGAGATGCGA GGGTCCAATAC
P1-GAPDH	TTGGCTACAGCAACA-FAM
P2-PD-L1	AAAGTGATACACATT-Cy3
P3-CK	GCGGGTGGTTTGAGC-Cy5
GAPDH RNA	CGAAUUUGGCUACAGCAACA
PD-L1 RNA	GAAGCAAAGUGAUACACAUU
CK RNA	GCUAUGCGGGUGGUUUGAGC
GAPDH P-F	CTGGGCTACACTGAGCACC
GAPDH P-R	AAGTGGTCGTTGAGGGCAATG
PD-L1 P-F	TTTGCTGAACGCCCCATAC
PD-L1 P-R	TCTCAGTGTGCTGGTCACAT
CK P-F	ATTCATACGAAGACCACCGGC
CK P-R	TCACGTGTCTCGATCTTCTTC

Table S2. Electrical properties for simulation in COMSOL Multiphysics.

Material	Conductivity (S/m)	Relative dielectric constant
PBS	11.5	80
PET/PDMS	1×10^{-15}	2.9
Intercellular fluid	0.2	50
Cytoplasmic membrane/ nuclear membrane	5×10^{-7}	1

PBS, phosphate buffer saline. PET, polyethylene terephthalate. PDMS, polydimethylsiloxane.

Table S3. Information of NSCLC patients.

Patient ID	Age	Gender	Pathological subtype	cTNM stage	Total CTCs	PD-L1^{+} CTCs	PD-L1^{high} CTCs	PA^{+} CTCs	PD-L1^{high} & PA^{+} CTCs	PD-L1^{+} & PA^{+} CTCs	NICHE index /%
1	71	M	AC	IA	2	1	0	0	0	0	0.00
2	68	W	AC	IA	3	3	1	1	0	1	0.00
3	52	W	AC	IA	2	2	1	0	0	0	0.00
4	62	M	AC	IA	4	3	1	2	1	1	25.00
5	49	W	AC	IA	4	3	2	1	1	1	25.00
6	66	M	SC	IA	3	3	3	2	2	2	66.67
7	64	M	AC	IA	1	1	0	0	0	0	0.00
8	53	W	AC	IA	4	3	2	2	2	2	50.00
9	68	M	AC	IA	2	0	0	1	0	0	0.00
10	74	W	AC	IA	2	2	0	0	0	0	0.00
11	71	M	AC	IA	5	5	4	2	1	2	20.00
12	74	W	AC	IA	4	4	3	2	2	2	50.00
13	53	M	AC	IA	5	0	0	3	0	0	0.00
14	82	M	SC	IA	7	7	5	4	2	4	28.57
15	59	M	SC	IB	3	3	1	1	0	1	0.00
16	66	M	SC	IA	8	6	5	6	5	6	62.50
17	64	M	SC	IB	4	4	3	2	2	2	50.00
18	67	M	SC	IIB	2	2	2	1	1	1	50.00
19	77	W	AC	IIA	4	4	2	3	2	3	50.00
20	69	M	SC	IIA	3	3	2	1	1	1	33.33
21	71	W	AC	IIB	5	5	3	2	1	2	20.00
22	76	M	SC	IIB	7	7	6	6	6	6	85.71
23	69	M	SC	IIB	3	3	3	3	3	3	100.00
24	76	M	SC	IIB	4	4	4	3	3	3	75.00
25	64	M	SC	IIB	3	3	2	2	2	2	66.67
26	69	M	SC	IIB	2	2	1	2	1	2	50.00
27	53	M	SC	IIB	6	6	6	5	5	5	83.33
28	61	M	SC	IIB	5	5	4	4	4	4	80.00
29	55	W	AC	IIB	3	3	2	3	2	3	66.67
30	56	W	SC	IIB	6	6	3	3	2	3	33.33
31	64	M	SC	IIB	3	3	1	2	1	2	33.33
32	66	M	SC	IIIA	8	8	6	4	4	4	50.00
33	49	M	SC	IIIB	7	5	4	2	0	1	0.00
34	49	M	SC	IIIB	4	4	4	4	4	4	100.00
35	67	M	AC	IIIA	9	9	4	5	3	5	33.33
36	55	M	AC	IIIA	7	7	7	7	7	7	100.00
37	64	W	SC	IIIA	4	2	1	3	0	1	0.00
38	57	M	SC	IIIA	8	8	7	7	7	7	87.50
39	67	M	AC	IIIA	4	4	4	4	4	4	100.00
40	61	M	SC	IIIA	5	5	2	3	1	3	20.00
41	61	M	SC	IIIA	7	7	6	6	6	6	85.71
42	51	M	SC	IIIA	11	11	11	11	11	11	100.00
43	60	M	AC	IIIA	6	3	2	2	0	2	0.00
44	40	M	SC	IIIA	15	15	15	10	10	10	66.67
45	60	M	SC	IIIA	11	11	10	10	10	10	90.91
46	77	M	SC	IIIB	13	13	12	10	10	10	76.92
47	70	M	SC	IIIA	9	9	8	8	8	8	88.89
48	55	M	SC	IIIB	5	5	5	5	5	5	100.00
49	66	M	AC	IIIA	8	5	5	4	4	4	50.00
50	58	M	SC	IIIA	13	13	7	10	7	10	53.85
51	60	M	SC	IIIB	11	11	9	9	9	9	81.82
52	59	M	SC	IIIB	9	6	6	5	5	5	55.56
53	54	M	SC	IIIA	4	4	4	2	2	2	50.00
54	75	M	SC	IIIA	9	9	9	6	6	6	66.67

55	83	M	SC	IIIA	10	6	6	5	4	5	40.00
56	63	M	SC	IIIA	8	8	6	4	4	4	50.00
57	70	M	AC	IIIA	7	4	4	4	3	4	42.86
58	69	M	SC	IIIB	15	15	12	11	10	11	66.67
59	72	M	AC	IIIA	9	6	6	8	6	6	66.67
60	57	M	SC	IIIB	18	18	18	15	15	15	83.33
61	52	M	SC	IIIB	8	8	8	7	7	7	87.50
62	69	W	AC	IIIA	7	4	4	5	4	4	57.14
63	59	M	SC	IIIB	10	10	8	7	7	7	70.00
64	68	M	SC	IIIB	5	5	4	4	4	4	80.00
65	67	M	SC	IIIA	7	7	3	5	2	5	28.57
66	64	M	SC	IIIA	14	14	12	14	12	14	85.71
67	67	W	AC	IV	9	9	8	4	3	4	33.33
68	63	W	AC	IV	11	11	4	8	4	8	36.36
69	75	M	SC	IV	19	16	9	7	5	7	26.32
70	69	M	AC	IV	12	12	12	10	10	10	83.33
71	66	M	SC	IV	8	8	6	5	4	5	50.00
72	63	M	SC	IV	9	5	2	6	2	5	22.22
73	67	M	SC	IV	7	7	7	5	5	5	71.43
74	66	M	SC	IV	11	10	7	8	6	8	54.55
75	66	M	AC	IV	13	13	10	8	8	8	61.54
76	69	M	SC	IV	8	8	8	6	6	6	75.00
77	73	M	SC	IV	7	7	5	7	5	7	71.43
78	63	M	AC	IV	16	14	11	14	11	14	68.75
79	60	M	AC	IV	9	6	5	7	5	6	55.56
80	49	M	AC	IV	7	3	0	5	0	3	0.00

W, woman. M, man. AC, adenocarcinoma. SC, squamous cell carcinoma.

Table S4. Information on NSCLC patients who underwent surgery after receiving immunotherapy.

Patient ID	Response evaluation	Residual tumor volume	TPS
16	pCR	0%	-
21	MPR-	12%	70%
22	pCR	0%	-
23	pCR	0%	95%
25	pCR	0%	-
26	MPR	1%	30%
29	pCR	0%	0%
30	MPR	5%	0%
32	MPR	2%	40%
33	MPR-	13%	0%
34	pCR	0%	10%
36	pCR	0%	60%
37	MPR-	50%	-
38	pCR	0%	80%
39	pCR	0%	2%
40	pCR	0%	15%
41	pCR	0%	-
42	pCR	0%	-
44	pCR	0%	-
45	pCR	0%	-
47	pCR	0%	5%
48	pCR	0%	75%
49	MPR-	70%	0%
50	MPR	5%	0%
51	pCR	0%	-
52	MPR	3.4%	65%
55	pCR	0%	1%
56	-	0%	1%
59	pCR	0%	100%
61	pCR	5%	100%
62	MPR	0%	85%
63	pCR	0%	60%
64	pCR	32%	70%
65	MPR-	0%	45%
66	pCR	0%	1%

pCR, pathologic complete response. MPR, major pathological remission. MPR-, major pathological remission is not achieved. TPS, tumor proportion score.

Table S5. Information on NSCLC patients who have not undergone surgery after receiving immunotherapy.

Patient ID	Response evaluation	TPS
17	-	-
24	PR	95%
27	PR	-
28	PR	70%
31	SD	10%
35	SD	-
46	-	-
53	SD	30%
54	PR	0%
57	PR	35%
58	PR	-
60	PR	0%
67	-	-
68	-	-
69	PD	60%
70	-	-
71	SD	80%
72	PD	0%
73	PR	-
74	-	0%
75	PR	0%
76	-	70%
77	-	-
78	PR	-
79	SD	-
80	PD	-

PR, partial response. SD, stable disease. PD, progressive disease.

Table S6. Information of NSCLC patients in training cohort.

Patient ID	Response evaluation	Residual tumor volume	TPS	PD-L1^{+}	PA^{+}	PD-L1^{high}	PD-L1^{+} & PA^{+}	PD-L1^{high} & PA^{+}
16	pCR	0%	-	75.00	75.00	62.50	75.00	62.50
23	pCR	0%	95%	100.00	100.00	100.00	100.00	100.00
26	MPR	1%	30%	100.00	100.00	50.00	100.00	50.00
27	PR	-	-	100.00	83.33	100.00	83.33	83.33
28	PR	-	70%	100.00	80.00	80.00	80.00	80.00
30	MPR	5%	0%	100.00	50.00	50.00	50.00	33.33
31	SD	-	10%	100.00	66.67	33.33	66.67	33.33
34	pCR	0%	10%	100.00	100.00	100.00	100.00	100.00
37	MPR-	50%	-	50.00	75.00	25.00	25.00	0.00
38	pCR	0%	80%	100.00	87.50	87.50	87.50	87.50
39	pCR	0%	2%	100.00	100.00	100.00	100.00	100.00
42	pCR	0%	-	100.00	100.00	100.00	100.00	100.00
45	pCR	0%	-	100.00	90.91	90.91	90.91	90.91
48	pCR	0%	75%	100.00	100.00	100.00	100.00	100.00
49	MPR-	70%	0%	62.50	50.00	62.50	50.00	50.00
53	SD	-	30%	100.00	50.00	100.00	50.00	50.00
55	pCR	0%	1%	60.00	50.00	60.00	50.00	40.00
57	PR	-	35%	57.14	57.14	57.14	57.14	42.86
59	pCR	0%	100%	66.67	88.89	66.67	66.67	66.67
60	PR	-	0%	100.00	83.33	100.00	83.33	83.33
62	MPR	0%	85%	57.14	71.43	57.14	57.14	57.14
64	pCR	32%	70%	100.00	80.00	80.00	80.00	80.00
66	pCR	0%	1%	100.00	100.00	85.71	100.00	85.71
71	SD	-	80%	100.00	62.50	75.00	62.50	50.00
78	PR	-	-	87.50	87.50	68.75	87.50	68.75
80	PD	-	-	42.86	71.43	0.00	42.86	0.00

pCR, pathologic complete response. MPR, major pathological remission. MPR-, major pathological remission is not achieved. TPS, tumor proportion score. PR, partial response. SD, stable disease. PD, progressive disease.

Table S7. Information of NSCLC patients in validation cohort.

Patient ID	Response evaluation	Residual tumor volume	TPS	PD-L1^{+}	PA^{+}	PD-L1^{high}	PD-L1^{+} & PA^{+}	PD-L1^{high} & PA^{+}
21	MPR-	12%	70%	100.00	40.00	60.00	40.00	20.00
22	pCR	0%	-	100.00	85.71	85.71	85.71	85.71
24	PR	-	95%	100.00	75.00	100.00	75.00	75.00
25	pCR	0%	-	100.00	66.67	66.67	66.67	66.67
29	pCR	0%	0%	100.00	100.00	66.67	100.00	66.67
32	MPR	2%	40%	100.00	50.00	75.00	50.00	50.00
33	MPR-	13%	0%	71.43	28.57	57.14	14.29	0.00
35	SD	-	-	100.00	55.56	44.44	55.56	33.33
36	pCR	0%	60%	100.00	100.00	100.00	100.00	100.00
40	pCR	0%	15%	100.00	60.00	40.00	60.00	20.00
41	pCR	0%	-	100.00	85.71	85.71	85.71	85.71
44	pCR	0%	-	100.00	66.67	100.00	66.67	66.67
47	pCR	0%	5%	100.00	88.89	88.89	88.89	88.89
50	MPR	5%	0%	100.00	76.92	53.85	76.92	53.85
51	pCR	0%	-	100.00	81.82	81.82	81.82	81.82
52	MPR	3.4%	65%	66.67	55.56	66.67	55.56	55.56
54	PR	-	0%	100.00	66.67	100.00	66.67	66.67
58	PR	-	-	100.00	73.33	80.00	73.33	66.67
61	pCR	5%	100%	100.00	87.50	100.00	87.50	87.50
63	pCR	0%	60%	100.00	70.00	80.00	70.00	70.00
65	MPR-	0%	45%	100.00	71.43	42.86	71.43	28.57
69	PD	-	60%	84.21	36.84	47.37	36.84	26.32
72	PD	-	0%	55.56	66.67	22.22	55.56	22.22
73	PR	-	-	100.00	71.43	100.00	71.43	71.43
75	PR	-	0%	100.00	61.54	76.92	61.54	61.54
79	SD	-	-	66.67	77.78	55.56	66.67	55.56

pCR, pathologic complete response. MPR, major pathological remission. MPR-, major pathological remission is not achieved. TPS, tumor proportion score. PR, partial response. SD, stable disease. PD, progressive disease.

Table S8. Comparison of parameter performance in training cohort.

Parameter	AUC	Sensitivity	Specificity	Jordon index	Optimal threshold
$PDL1^{+}$	0.624	88.2%	44.4%	0.327	66.667
PA^{+}	0.83	82.4%	88.9%	0.712	80
$PDL1^{high}$	0.859	94.1%	66.7%	0.608	60
$PDL1^{+}\&PA^{+}$	0.859	82.4%	88.9%	0.712	75
$PDL1^{high}\&PA^{+}$	0.935	88.2%	100%	0.882	62.5

Table S9. Actual response and predicted response in validation cohort.

Patient ID	Actual	PD-L1^{+}	PA^{+}	PD-L1^{high}	PD-L1^{+} & PA^{+}	PD-L1^{high} & PA^{+}
21	Low	High	Low	High	Low	Low
22	High	High	High	High	High	High
24	High	High	Low	High	High	High
25	High	High	Low	High	Low	High
29	High	High	High	High	High	High
32	Low	High	Low	High	Low	Low
33	Low	High	Low	Low	Low	Low
35	Low	High	Low	Low	Low	Low
36	High	High	High	High	High	High
40	High	High	Low	Low	Low	Low
41	High	High	High	High	High	High
44	High	High	Low	High	Low	High
47	High	High	High	High	High	High
50	Low	High	Low	Low	High	Low
51	High	High	High	High	High	High
52	Low	High	Low	High	Low	Low
54	High	High	Low	High	Low	High
58	High	High	Low	High	Low	High
61	High	High	High	High	High	High
63	High	High	Low	High	Low	High
65	Low	High	Low	Low	Low	Low
69	Low	High	Low	Low	Low	Low
72	Low	Low	Low	Low	Low	Low
73	High	High	Low	High	Low	High
75	High	High	Low	High	Low	Low
79	Low	High	Low	Low	Low	Low

Table S10. Information of NSCLC patients for treatment monitoring.

Patient ID	Response evaluation	Sampling frequency	1		2		3		4	
			Number of CTCs	NICHE index/%	Number of CTCs	NICHE Index/%	Number of CTCs	NICHE Index/%	Number of CTCs	NICHE Index/%
16	pCR	3	8	62.50	4	75.00	2	100.00	-	-
21	MPR-	4	5	20.00	3	33.33	4	25.00	3	33.33
22	pCR	3	7	85.71	5	60.00	2	100.00	-	-
23	pCR	3	3	100.00	2	100.00	1	100.00	-	-
24	PR	3	4	75.00	2	100.00	2	100.00	-	-
25	pCR	3	3	66.67	1	100.00	0	-	-	-
26	MPR	3	2	50.00	2	50.00	1	0.00	-	-
27	PR	3	6	83.33	4	75.00	2	50.00	-	-
30	MPR	3	6	33.33	5	40.00	4	25.00	-	-
50	MPR	3	13	53.84	7	42.86	5	20.00	-	-
51	pCR	4	11	81.82	7	85.71	5	80.00	2	100.00
52	MPR	3	9	55.56	6	33.33	5	20.00	-	-
59	pCR	3	9	66.67	4	75.00	2	50.00	-	-
62	MPR	3	7	57.14	6	50.00	4	50.00	-	-
63	pCR	4	10	70.00	5	80.00	2	100.00	1	100.00
66	pCR	3	14	85.71	8	75.00	4	75.00	-	-

Movie Captions:

Movie S1. WBC removal inlet. The inlet area of the microfluidic chip, at the entrance of the WBC removal layer. The cells are flowing into the layer at the bottom of the video pushed by the buffer inlet on the top.

Movie S2: WBC removal through magnetic force. shows the WBC removal functionality (further from the area of Movie S1). Cells flow at the bottom of the channel when the magnet is off. When it is turned on, the labeled WBCs are attracted to the top of the channel.

Movie S3: WBC removal outlet. shows the outcome of the WBC removal (futher from the area of Movie S2). Cells that were deflected are exiting the channel on the top outlet, whilst unaffected cells can be seen leaving the channel by the bottom inlet.

Movie S4: CTC-capture. Demonstrates the CTC-capture functionality, with a single cell being trapped in the highlighted “micro-fence”.

Movie S5: NEED function. shows a fluorescent observation of a cell trapped in the capture layer (artificially recolored in red for ease of referencing), undergoing the NEED treatment to incorporate a cy5-DNAT probe.

Movie S6: Cell morphology – elongated. shows a single cell tagged with DiO, overlayed with a brightfield image showing the elongation after stimulation over 72h.

Movie S7: Cell morphology – no elongation. Same condition as Movie S6 but with an unstimulated cell, which does not change in morphology.

Movie S8: Cell morphology – control. Same condition as Movies S6 and S7 as a control (no activation).

The interval between two frames is 120 seconds in Movie S6, Movie S7 and Movie S8. The other movies are provided with the actual playing speed.